

Supporting Information

Aggregation and deposition behaviors of dissolved black carbon with coexisting heavy metals in aquatic solution

Yanghui Xu[†], Qin Ou[†], Caihong Liu[†], Xiaojun Zhou[†], Qiang He[†], Zhengsong Wu[†],
Ruixing Huang[†], Jun Ma[‡], Dongming Lu[§], Xiaoliu Huangfu^{*†}

[†]Key Laboratory of Eco-environments in Three Gorges Reservoir Region, Ministry of Education, College of Environment and Ecology, Chongqing University 400044, China

[‡]State Key Laboratory of Urban Water Resource and Environment, School of Municipal and Environmental Engineering, Harbin Institute of Technology 150001, China

[§]Xining Water Supply (Group) Co., Ltd 810000, China

*Corresponding authors email:

Dr. Xiaoliu Huangfu hfxl@cqu.edu.cn

Tel: +86-023-6512-0980

Fax: +86-023-6512-0980

Summary: 4 texts, 1 tables, and 13 figures

Text S1. QCM-D crystal sensor cleaning methods (referring to Cleaning & Immobilization Protocols in User's guides)

1. QSX 303 Silicon Dioxide and QSX 309 Aluminum Oxide

- a. UV/ozone treatment for 20 minutes.
- b. Immerse the sensor surface in the solution of 2% SDS for 30 min in room temperature.
- c. Rinse with DDI water and dry with nitrogen gas.
- d. UV/ozone treatment for 20 minutes.

Note that for crystal sensors used in coated surfaces deposition experiments, the crystal sensors were immersed in 1% Hellmanex II instead of 2% SDS solution.

Test S2. Characterization of the deposited films.

The atomic force microscope (AFM) and scanning electron microscopy (SEM) techniques were applied to characterize the surface morphology and roughness of the deposited films. The film samples need to prepare before the experiments. The silica surfaces were first immersed in background cationic solution, and then exposed to DBC solutions with same cation concentration for 1 h. The adsorbed layers were carefully took out of the solutions and dried in clean air (25 °C) to harvest the samples.

AFM was performed with a multimode scanning probe microscope (Dimension EDGE, Bruker, Germany) and the images were scanned in tapping mode using silicon cantilevers ($k = 4 \text{ N/m}$, 8 nm nominal tip radius). No image processing except flattening was made. The scanned image size was $25 \mu\text{m} \times 25 \mu\text{m}$. All experiments were conducted in a class-100 clean room at 25 °C. For each sample, images were acquired at multiple sample points (typically more than four regions).

After the AFM measurements, the samples were required to be coated with gold dust to further characterize the surface morphology using SEM. FEI Helios 650 Focused Ion Beam (FIB) SEM was used to collect SEM images (25 °C). All images were collected at 5 kV, 50 pA electron beam condition in a through-the-lens detector in backscatter mode. Two kinds of SEM images ($20000\times$, bar = 1 μm and $50000\times$, bar = 100 nm) were obtained to characterize the characteristic of each sample, at least 5 images were obtained per condition.

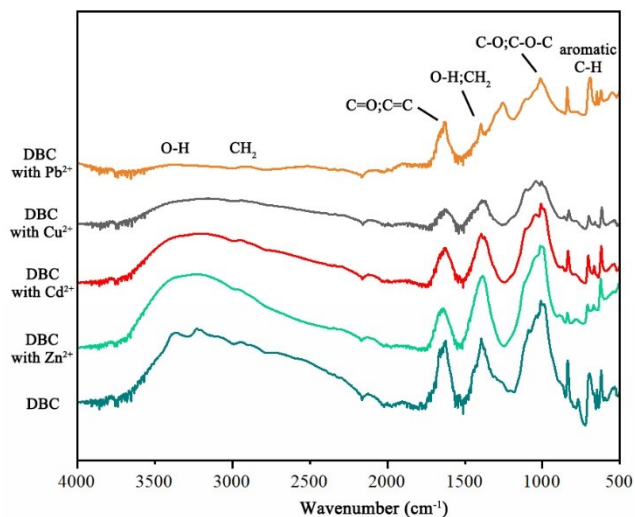


Fig. S1. FTIR spectra of DBC with and without heavy metals.

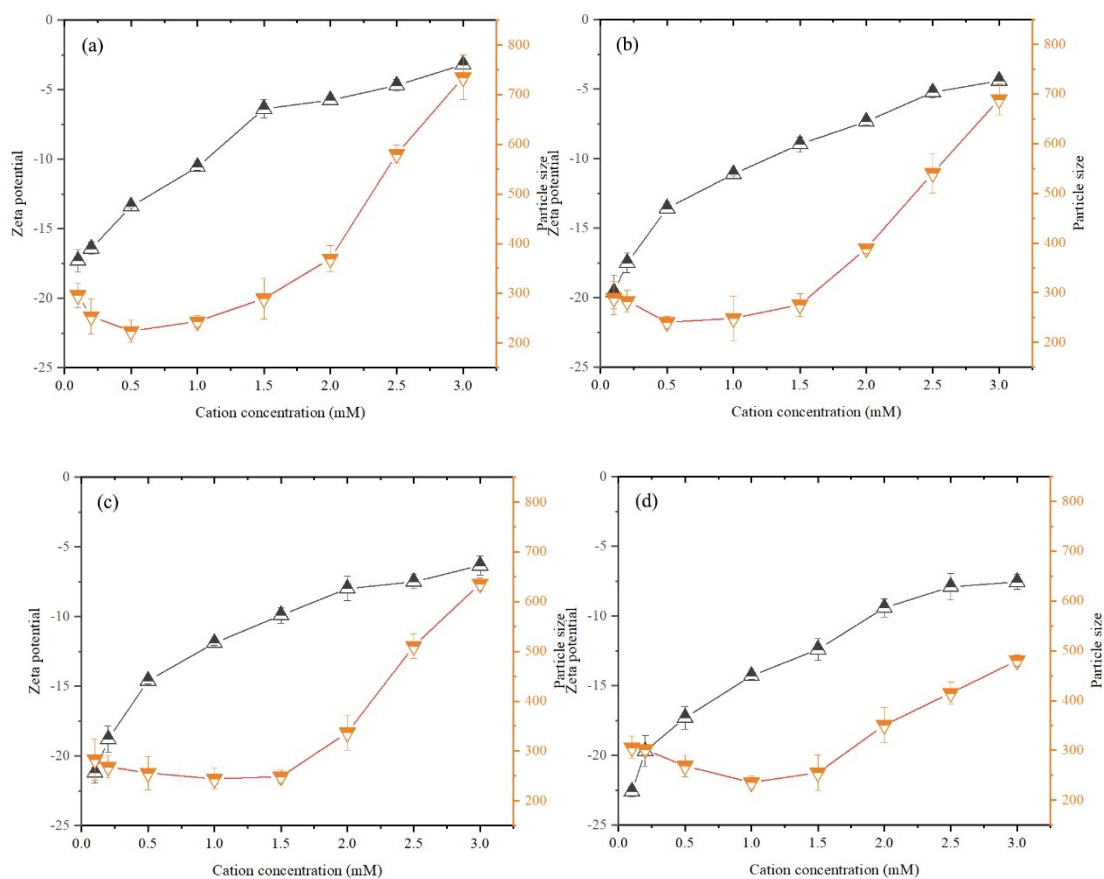


Fig. S2. The zeta potential (black upper triangles) and particle size (yellow inverted triangles) changes of DBC as a function of Pb^{2+} concentration (a), Cu^{2+} concentration (b), Cd^{2+} concentration (c), and Zn^{2+} concentration (d).

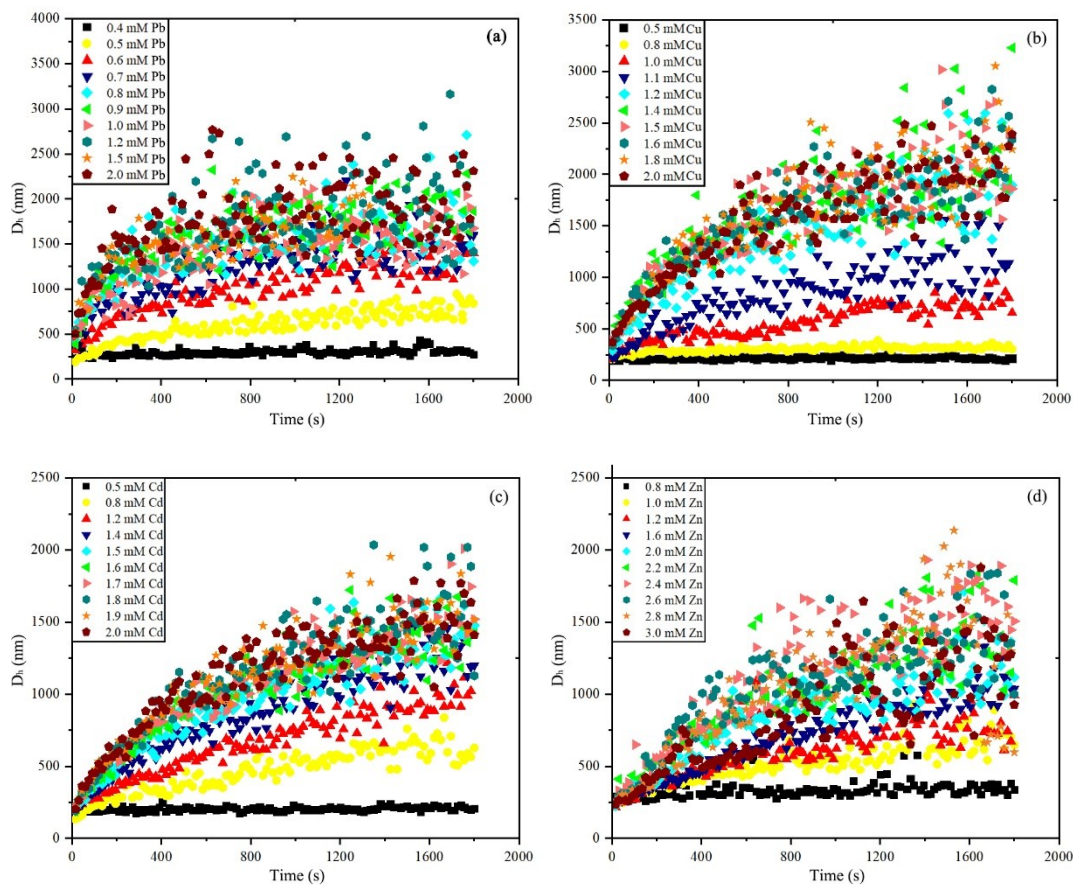


Fig. S3. Typical aggregation kinetics of DBC at different Pb^{2+} concentration (a), Cu^{2+} concentration (b), Cd^{2+} concentration (c), and Zn^{2+} concentration (d).

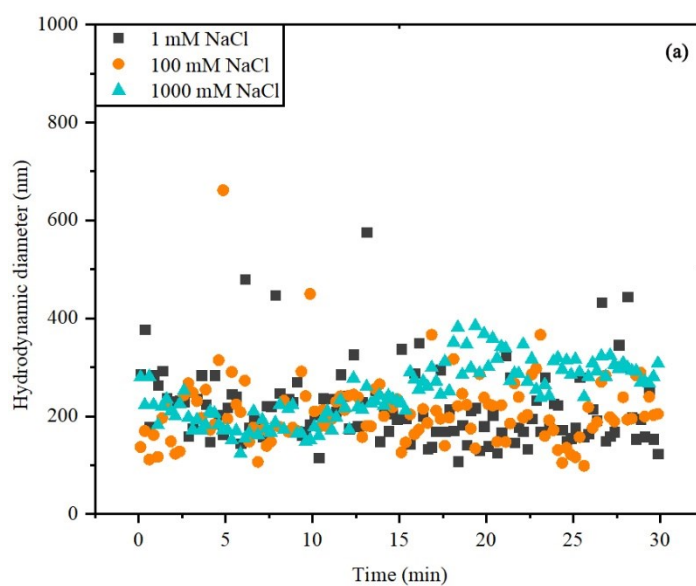


Fig. S4. Hydrodynamic diameter of DBC under NaCl solutions as a function of time.

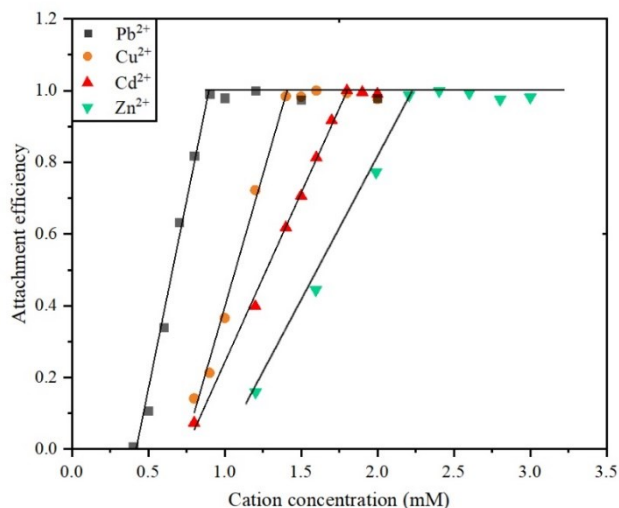


Fig. S5. Aggregation attachment efficiency of DBC as a function of cation concentration.

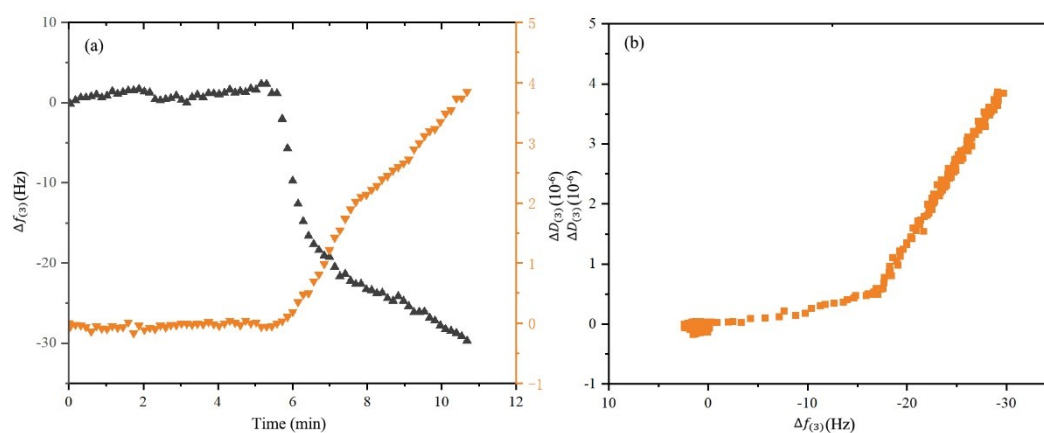


Fig. S6. (a). Representative frequency and dissipation shifts (from the third overtone measurements) for the deposition of DBC on the SiO₂ surface under 1 mM Cu²⁺ solution. Data present frequency shifts, $\Delta f_{(3)}$, black upper triangles, and dissipation shifts, $\Delta D_{(3)}$, yellow inverted triangles. (b). $\Delta D_{(3)}$ versus $\Delta f_{(3)}$ plot of the deposition of DBC under 1 mM Cu²⁺ solution.

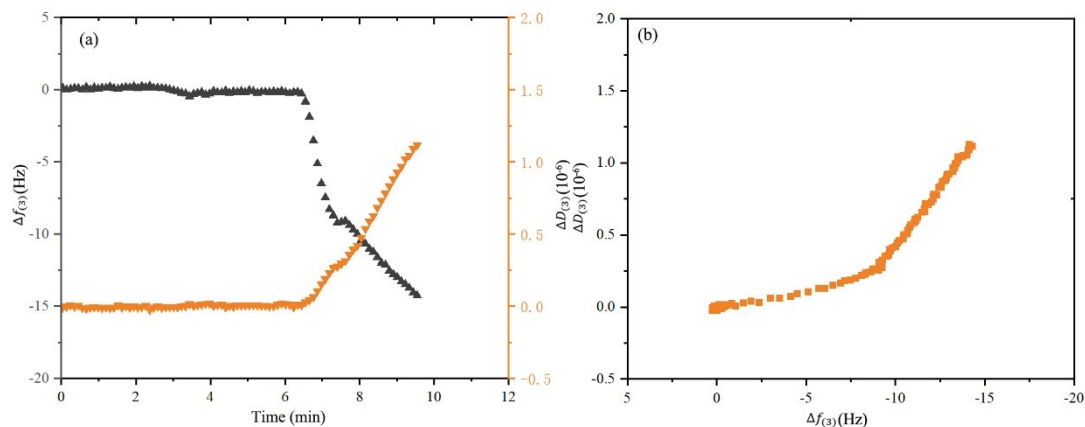


Fig. S7. (a). Representative frequency and dissipation shifts (from the third overtone measurements) for the deposition of DBC on the SiO_2 surface under 1 mM Cd^{2+} solution. Data present frequency shifts, $\Delta f_{(3)}$, black upper triangles, and dissipation shifts, $\Delta D_{(3)}$, yellow inverted triangles. (b). $\Delta D_{(3)}$ versus $\Delta f_{(3)}$ plot of the deposition of DBC under 1 mM Cd^{2+} solution.

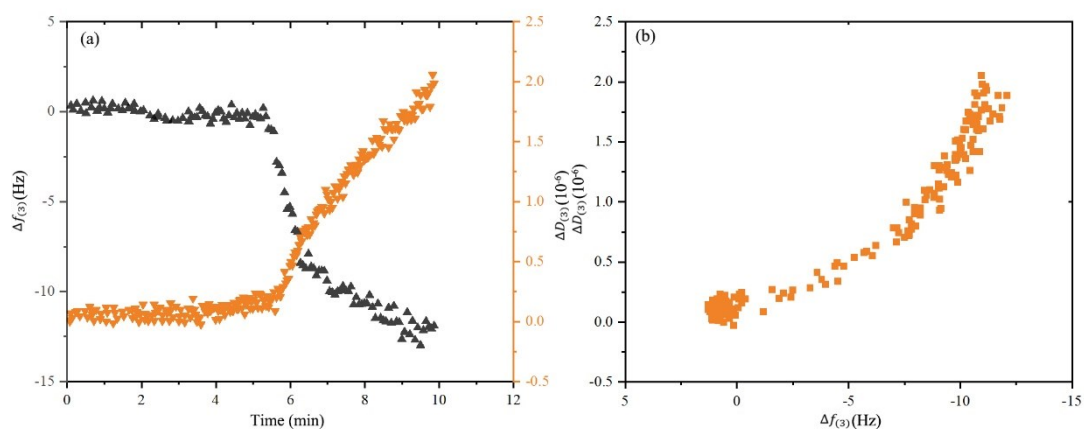


Fig. S8. (a). Representative frequency and dissipation shifts (from the third overtone measurements) for the deposition of DBC on the SiO_2 surface under 1 mM Zn^{2+} solution. Data present frequency shifts, $\Delta f_{(3)}$, black upper triangles, and dissipation shifts, $\Delta D_{(3)}$, yellow inverted triangles. (b). $\Delta D_{(3)}$ versus $\Delta f_{(3)}$ plot of the deposition of DBC under 1 mM Zn^{2+} solution.

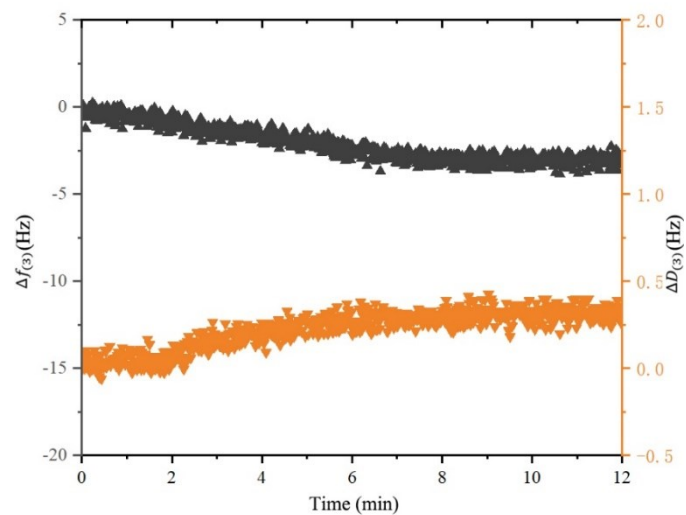


Fig. S9. Representative frequency and dissipation shifts (from the third overtone measurements) for the deposition of only DBC on the SiO_2 surface. Data present frequency shifts, $\Delta f_{(3)}$, black upper triangles, and dissipation shifts, $\Delta D_{(3)}$, yellow inverted triangles.

Text S3. Contact angle measurements and interfacial energy calculations

Contact angle measurement was determined to analyze the surface hydrophobicity of DBC under different water chemistry, as well as the tested silica surface. The sessile drop technique was employed to measure contact angles using a contact angle analyzer.¹ For DBC samples, 60 mL of prepared DBC solution (30 mg/L) with different water chemistry was filtered on a 0.22 μm cellulosic membrane. The formed layer was washed twice with desired salt solutions and then placed on 1% agar plate.¹ Before each measurement, the membrane was mounted on a glass slide with double faced adhesive tape and dried using nitrogen gas. The drops of water, formamide and diiodomethane were formed on samples surfaces applying the sessile-drop methods, and the contact angles of the liquid drops were determined by an image analysis attachments including video camera, monitor and image-analysis software.^{2, 3} All the contact angles of samples were measured at least five times to obtain means.

The contact angles measurement of three liquids (water, diiodomathane and formamide) aims to obtain the surface tension components and parameters of DBC and silica surface according to the extended Young's equation:⁴

$$(1 + \cos \theta)\gamma_L^{Tot} = 2\left(\sqrt{\gamma_L^{LW}\gamma_D^{LW}} + \sqrt{\gamma_L^-\gamma_D^+} + \sqrt{\gamma_L^+\gamma_D^-}\right) \quad (S1)$$

Where γ_L^{Tot} , γ_L^{LW} , γ_L^- , γ_L^+ are liquid surface tension, an apolar Liftshitz-van der Waals component, electron-donor and electron-acceptor parameters of a polar acid-base component. γ_D^{LW} , γ_D^- , γ_D^+ and γ_S^{LW} , γ_S^- , γ_S^+ are the surface tension components and parameters of DBC and silica surface, which can be obtained from equation (S1).

The interfacial free energy is a sum of van der Waals interaction energy (ΔG_{D-W-S}^{LW}) and Lewis acid-base interaction energy (ΔG_{D-W-S}^{AB}):

$$\Delta G_{D-W-S}^{adh} = \Delta G_{D-W-S}^{LW} + \Delta G_{D-W-S}^{AB} \quad (S2)$$

The interfacial free energy generated by van der Waals interaction (ΔG_{D-W-S}^{LW}) between DBC and silica surface can be calculated as follows:

$$\Delta G_{D-W-S}^{LW} = -2(\sqrt{\gamma_D^{LW}} - \sqrt{\gamma_W^{LW}})(\sqrt{\gamma_S^{LW}} - \sqrt{\gamma_W^{LW}}) \quad (S3)$$

The interfacial free energy generated by Lewis acid-base interaction (ΔG_{D-W-S}^{AB}) can be written as:

$$\begin{aligned} \Delta G_{D-W-S}^{AB} &= 2[\sqrt{\gamma_W^+}(\sqrt{\gamma_D^-} + \sqrt{\gamma_S^-} - \sqrt{\gamma_W^-}) + \sqrt{\gamma_W^-}(\sqrt{\gamma_D^+} + \sqrt{\gamma_S^+} - \sqrt{\gamma_W^+})] - \\ & \quad (S4) \end{aligned}$$

Table S1. Contact angle, Surface tension components, the van der Waals interaction energy (ΔG^{LW}), the Lewis acid-base interaction free energy (ΔG^{AB}) of DBC-silica and DBC-DBC systems.

Properties		Pb ²⁺	Cu ²⁺	Cd ²⁺	Zn ²⁺
Contact angle (°)	Water	67.11	64.40	63.11	62.34
	formamide	47.10	44.48	43.15	42.80
	diiodomethane	64.88	65.12	66.30	66.87
Surface tension components (mJ m ⁻²)	γ^{LW}	25.77	25.63	24.96	24.64
	γ^+	3.55	3.99	4.48	4.61
	γ^-	11.80	13.28	13.93	14.57
ΔG_{D-W-S}^{LW} (mJ m ⁻²)		-1.62	-1.57	-1.30	-1.17
ΔG_{D-W-S}^{AB} (mJ m ⁻²)		1.16	2.60	2.80	3.49
ΔG_{D-W-D}^{LW} (mJ m ⁻²)		-0.33	-0.31	-0.21	-0.17

ΔG_{D-W-D}^{AB} (mJ m ⁻²)	-20.45	-17.16	-15.46	-14.31
---	--------	--------	--------	--------

Text S4. The XDLVO interaction energy

The XDLVO theory was employed to calculate the interaction energy between DBC, as well as DBC and silica surface.^{5, 6}

$$E_{D-W-S}^{XDLVO} = E_{D-W-S}^{LW} + E_{D-W-S}^{AB} + E_{D-W-S}^{EL} \quad (S5)$$

$$E_{D-W-D}^{XDLVO} = E_{D-W-D}^{LW} + E_{D-W-S}^{AB} + E_{D-W-D}^{EL} \quad (S6)$$

$$E_{D-W-S}^{LW} = -\frac{A_1 R}{6h \left(1 + \frac{14h}{\lambda_0}\right)} \quad (S7)$$

$$E_{D-W-D}^{LW} = -\frac{A_2 R}{12h \left(1 + \frac{14h}{\lambda_0}\right)} \quad (S8)$$

$$E_{D-W-S}^{EL} = 64\pi\epsilon_0\epsilon_r R \left(\frac{k_B T}{ze}\right)^2 \Gamma_1 \Gamma_2 e^{(-\kappa h)} \quad (S9)$$

$$E_{D-W-D}^{EL} = 32\pi\epsilon_0\epsilon_r R \left(\frac{k_B T}{ze}\right)^2 \Gamma_1^2 e^{(-\kappa h)} \quad (S10)$$

$$E_{D-W-S}^{AB} = 2\pi R \lambda \Delta G_{D-W-S}^{AB} e^{-\frac{h_0 - h}{\lambda}} \quad (S11)$$

$$E_{D-W-D}^{AB} = \pi R \lambda \Delta G_{D-W-D}^{AB} e^{-\frac{h_0 - h}{\lambda}} \quad (S12)$$

Where E_{D-W-S}^{XDLVO} , E_{D-W-S}^{LW} , E_{D-W-S}^{EL} , E_{D-W-S}^{AB} and E_{D-W-D}^{XDLVO} , E_{D-W-D}^{LW} , E_{D-W-D}^{EL} , E_{D-W-D}^{AB} are the XDLVO interaction energy, the Lifshitz-van der Waals interaction energy, the electrostatic interaction energy and the Lewis acid-base interaction energy between DBC and silica surface, as well as between DBC in water.

Subscripts D , W , S stand for DBC, water and silica surface. R is the radius of DBC, $\epsilon_0\epsilon_r$ is the permittivity of medium ($6.95 \times 10^{-10} \text{ C}^2\text{J}^{-1}\text{m}^{-1}$), k_B is the Boltzmann-constant, T is the absolute temperature, z is the valence of ions, e is the electron charge, Γ_1 is the dimensionless surface potential of DBC, Γ_2 is the dimensionless surface potential of silica surface.⁷⁻⁹ κ^{-1} is the Debye screening length.³ λ_0 is the dielectric wavelength (100 nm), h is the separation between DBC and silica surface, λ is the characteristic decay length of AB interactions in water (0.6nm),⁴ A_1 and A_2 is the Hamaker constant for DBC-water-silica and DBC-water-DBC systems.

$$A_1 = -12\pi h_0^2 \Delta G_{D-W-S}^{LW} \quad (\text{S13})$$

$$A_2 = -12\pi h_0^2 \Delta G_{D-W-D}^{LW} \quad (\text{S14})$$

Where h_0 is the minimum equilibrium cut-off distance (distance where DBC contact the silica surface, 0.158nm), and ΔG_{D-W-S}^{LW} and ΔG_{D-W-D}^{LW} are the van der Waals interaction energies.

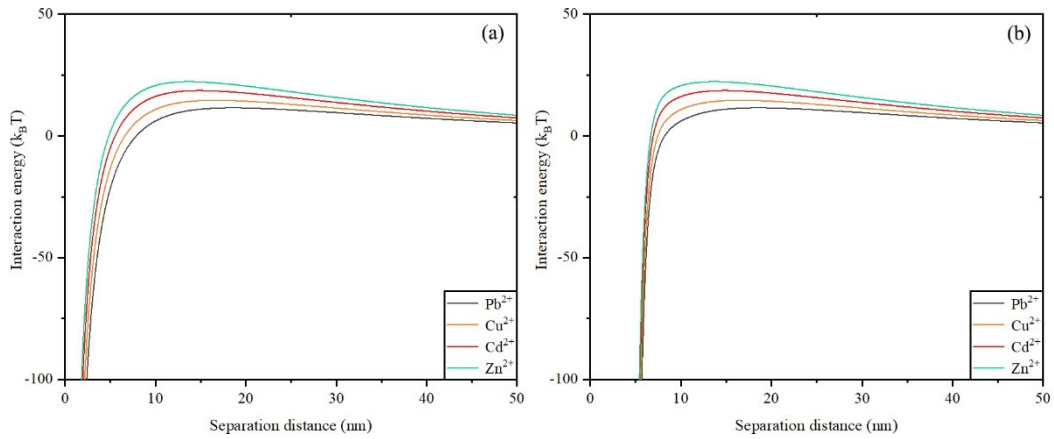


Fig. S10. The DLVO (a) and XDLVO (b) interaction energies between DBC in Pb^{2+} , Cu^{2+} , Cd^{2+} and Zn^{2+} solutions.

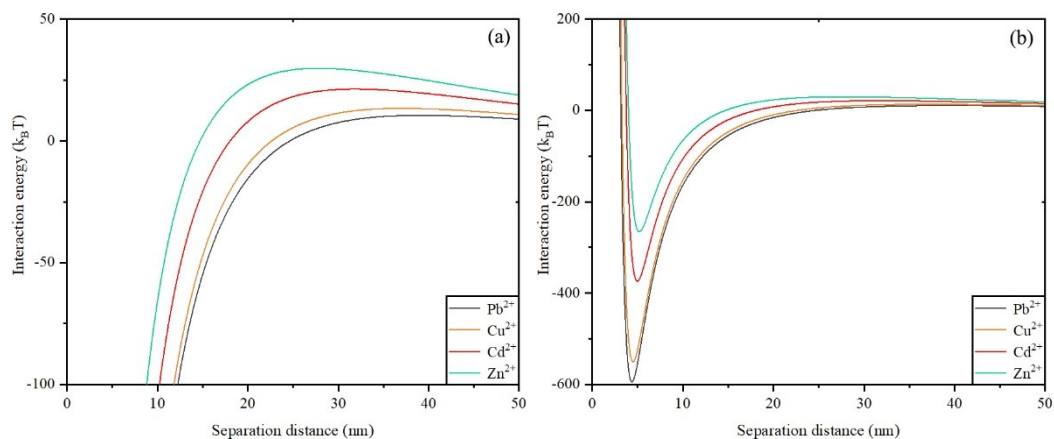


Fig. S11. The DLVO (a) and XDLVO (b) interaction energies between DBC and silica surface in Pb^{2+} , Cu^{2+} , Cd^{2+} and Zn^{2+} solutions.

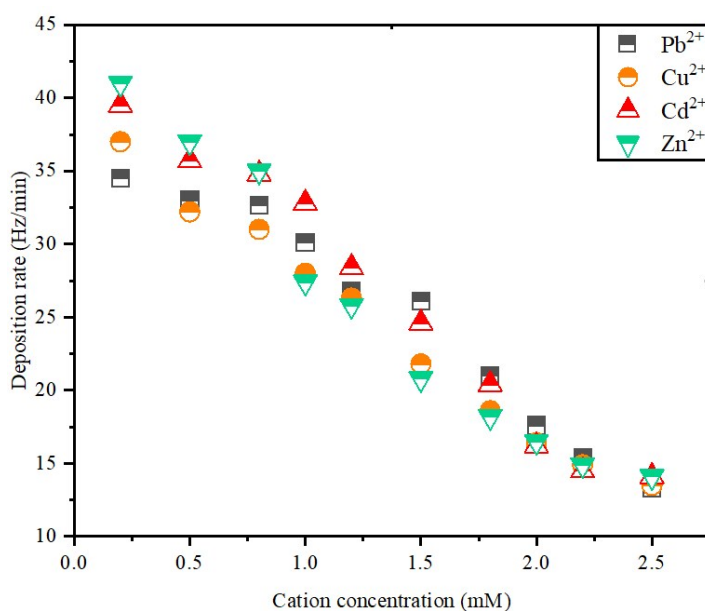
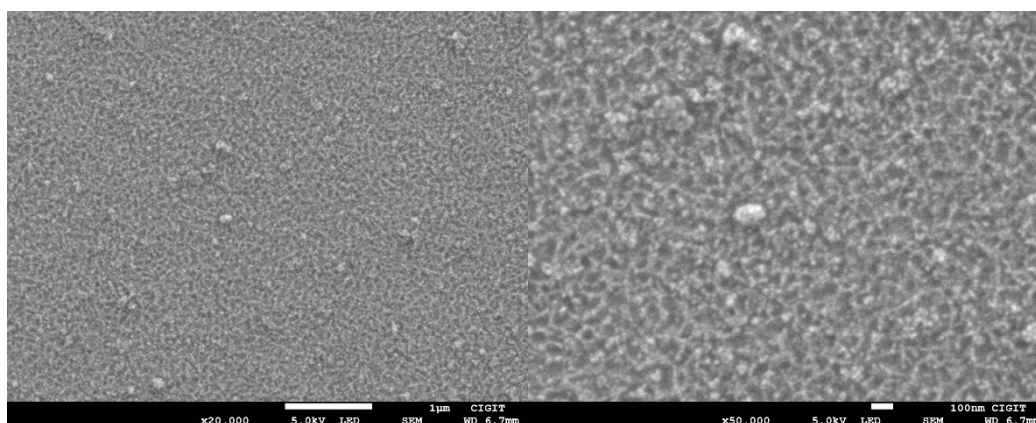
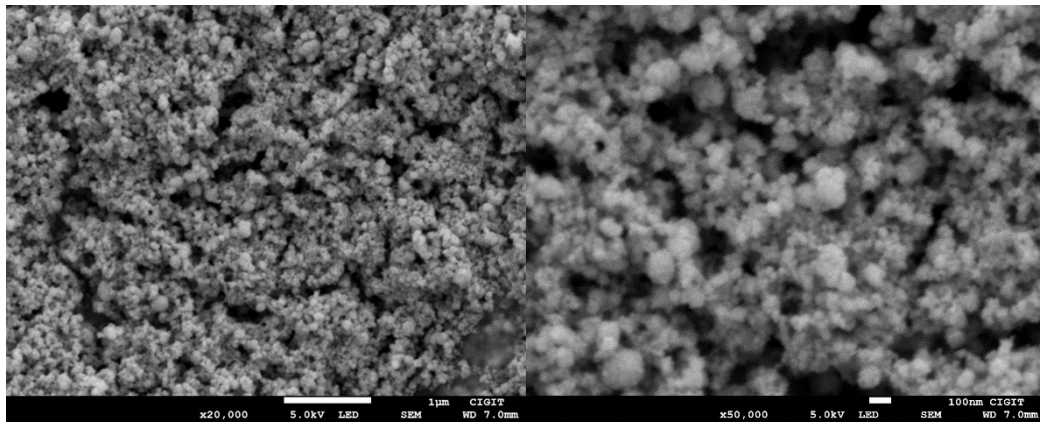


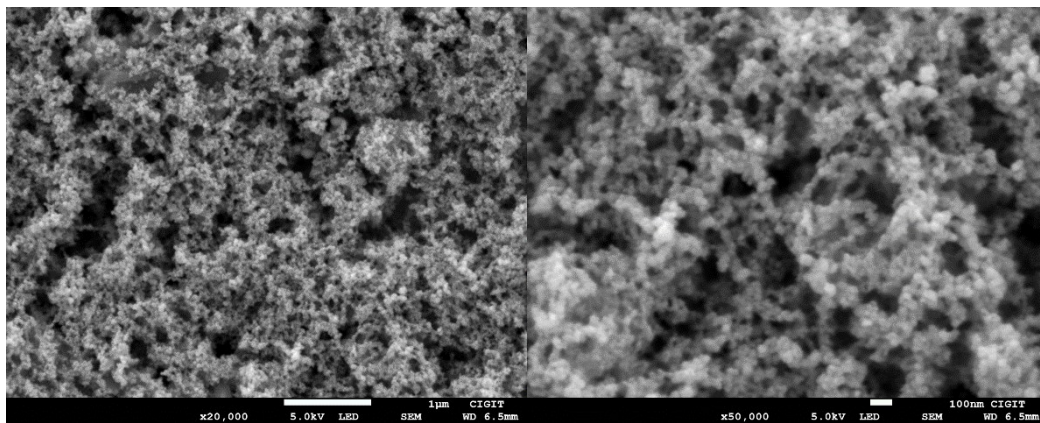
Fig. S12. The deposition rate of DBC on PLL coated silica surfaces under heavy metals of various cation concentrations.



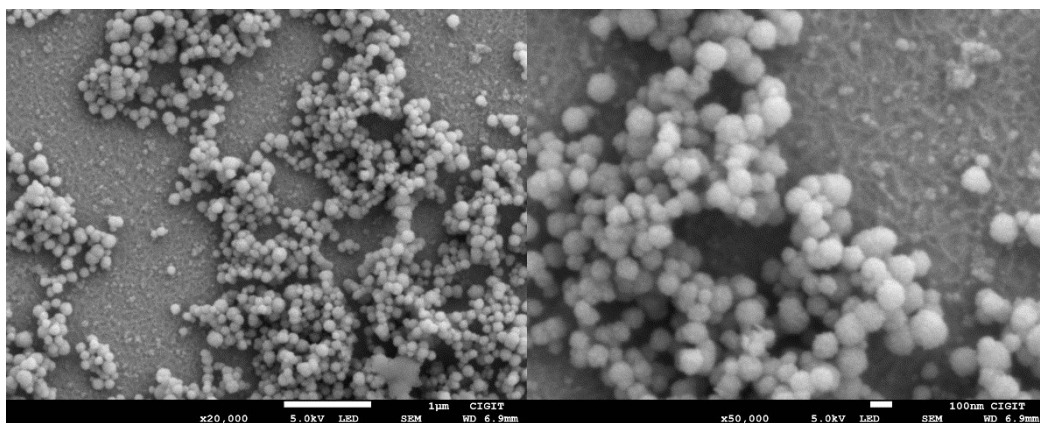
(a) Single DBC



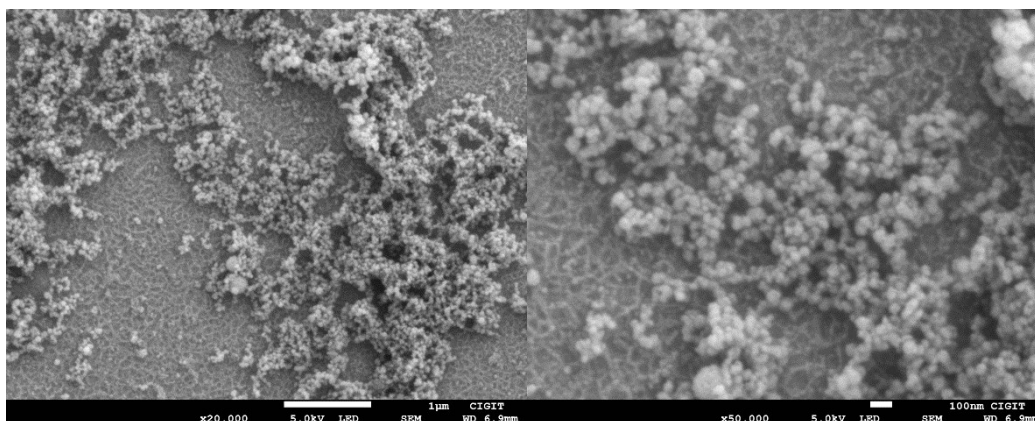
(b) DBC with Pb^{2+}



(c) DBC with Cu^{2+}



(d) DBC with Cd^{2+}



(e) DBC with Zn^{2+}

Fig. S13. SEM images of the deposited films. (a) Single DBC, (b) DBC with Pb^{2+} , (c) DBC with Cu^{2+} , (d) DBC with Cd^{2+} , and (e) DBC with Zn^{2+} .

References

1. Liu, X.-M.; Sheng, G.-P.; Yu, H.-Q., DLVO approach to the flocculability of a photosynthetic H_2 -producing bacterium, *Rhodospseudomonas acidophila*. *Environ. Sci. Technol* **2007**, *41* (13), 4620–4625.
2. Fu, W.; Wang, L.; Chen, F.; Zhang, X.; Zhang, W., Polyvinyl chloride (PVC) ultrafiltration membrane fouling and defouling behavior: EDLVO theory and interface adhesion force analysis. *Journal of Membrane Science* **2018**, *564*, 204-210.
3. Gao, F.; Wang, J.; Zhang, H.; Hang, M. A.; Cui, Z.; Yang, G., Interaction energy and competitive adsorption evaluation of different NOM fractions on aged membrane surfaces. *Journal of Membrane Science* **2017**, *542*, 195-207.
4. Lin, T.; Lu, Z.; Chen, W., Interaction mechanisms and predictions on membrane fouling in an ultrafiltration system, using the XDLVO approach. *Journal of Membrane Science* **2014**, *461*, 49-58.
5. Lin, S.; Wiesner, M. R., Theoretical investigation on the interaction between a soft particle and a rigid surface. *Chemical Engineering Journal* **2012**, *191*, 297-305.
6. Huangfu, X.; Ma, C.; Huang, R.; He, Q.; Liu, C.; Zhou, J.; Jiang, J.; Ma, J.; Zhu, Y.; Huang, M., Deposition Kinetics of Colloidal Manganese Dioxide onto Representative Surfaces in Aquatic Environments: The Role of Humic Acid and Biomacromolecules. *Environ Sci Technol* **2018**.
7. Kosmulski, M.; Dahlsten, P.; Próchniak, P.; Rosenholm, J. B., Electrokinetics at high ionic strengths: Alumina. *Colloids and Surfaces A: Physicochemical and Engineering Aspects* **2007**, *301* (1-3), 425-431.
8. Reyes Bahena, J. L.; Robledo Cabrera, A.; López Valdivieso, A.; Herrera Urbina, R., Fluoride adsorption onto $\alpha\text{-Al}_2\text{O}_3$ and its effect on the zeta potential at the alumina–aqueous electrolyte interface. *Separation Science and Technology* **2002**, *37* (8), 1973-1987.
9. Sondi, I.; Milat, O.; Pravdic, V., Electrokinetic Potentials of Clay Surfaces Modified by Polymers. *Journal of Colloid and Interface Science* **1997**, *189*, 66–73.

